A Ni(III) Mott-Hubbard-like State Containing High-Spin Ni(II) in a Semiconductive Bromide-Bridged Ni-Chain Compound

Masanori Wakizaka,[1,*] Mohammad Rasel Mian,[1] Takefumi Yoshida,[1] Tetsu Sato,[1] Hisaaki Tanaka,[2] Tatsuya Miyamoto,[3] Hiroshi Okamoto,[3,4] Shinya Takaishi,[1] Hiroaki Iguchi,[1] and Masahiro Yamashita[1,5,*]

[1] Department of Chemistry, Graduate School of Science, Tohoku University, 6-3 Aramaki-Aza-Aoba, Aoba-Ku, Sendai 980-8578, Japan. Fax: +81-22-795-6548; Tel: +81-22-795-6545.

[2] Department of Applied Physics, Graduate School of Engineering, Nagoya University, Chikusa-Ku, Nagoya 464-8603, Japan.

[3] Department of Advanced Material Science, Graduate School of Frontier Sciences, The University of Tokyo, Kashiwa 277-8561, Japan

[4] AIST-UTokyo Advanced Operando-Measurement Technology Open Innovation Laboratory, National Institute of Advanced Industrial Science and Technology, Chiba 277-8568, Japan

[5] School of Materials Science and Engineering, Nankai University, Tianjin 300350, P. R. China

E-mail: masanori.wakizaka.a7@tohoku.ac.jp, yamasita@agnus.chem.tohoku.ac.jp

Key Words: Mott-Hubbard, Mixed-valency, Nickel(III) complex, Charge density wave state, MX-Chains

Abstract

Halogen-bridged linear chain metal complexes (MX-Chains) are fascinating compounds that have a quasi-one-dimensional (1D) electronic system. Herein, this study synthesized the first Ni-based MX-Chain compound having hydroxy groups, i.e., $[Ni(dabdOH)_2Br]Br_2 \cdot [Ni(dabdOH_x)_2Br]_{0.5} \cdot (2\text{-}PrOH)_{0.25} \cdot (MeOH)_{0.25}$ (**1**·solvent, x = ~0.6, dabdOH = (2*S*,3*S*)-2,3-diaminobutane-1,4-diol). Single-crystal X-ray diffraction revealed that the MX-Chains in **1**·solvent formed sheets and single-chain structures in the superlattice. It suggested a MH-like state, whereas the polarized reflection and Raman spectra suggested a CDW-like state. Magnetic and electron spin resonance measurements revealed that both high-spin Ni(II) (~15%) and low-spin Ni(III) (~85%) sites are present in the chain structures, i.e., that the metal sites show mixed-valency. Therefore, we concluded that **1**·solvent adopts an intermediate state between the MH and CDW states. Moreover, a single crystal of **1**·solvent exhibited semiconductive characteristics along the chain direction. This finding represents a new structural and electronic state for 1D-electronic systems as well as MX-Chains.

Introduction

One-dimensional (1D) electronic systems are a fascinating research topic in both the materials chemistry and theoretical physics fields. Various types of (quasi-) 1D compounds and materials, e.g., fulvalenes,[1,2] metal dithiolene complexes,[3,4] single-walled carbon nanotubes[5–7] and others,[8] have been synthesized to date and found to exhibit unique conductive, optical, and magnetic properties.[9–12] In this context, halogen-bridged metal complexes (MX-Chains, $[M(A)_2X]Y_2$) are highly designable compounds with great flexibility in the choice of metal (M), in-plane ligand (A), bridging halide (X), and counter anions (Y).[13] An alternating linear structure composed of the d_z^2 orbitals on M and the p_z orbitals on X forms the 1D electronic system. Pd- and Pt-based MX-Chains have been reported to typically adopt the charge-density-wave (CDW) state or the mixed-valence state.[14,15] The mixed-valence states are diamagnetic M(II)/M(IV) or M(III–ρ)/M(III+ρ) states, which represent a type of disproportionation[16] and are caused by Peierls instability, which is characteristic of 1D electronic systems. On the other hand, Ni-based MX-Chains have been reported to adopt the Mott–Hubbard (MH) state with an average Ni(III) valence state.[17] According to the extended Peierls–Hubbard model,[18] the electron–electron interaction energy at the Ni sites, which exhibit strong electron-correlation, suppresses the electron–phonon interaction energy, resulting in the stabilization of the Ni(III) MH state.

However, the first example of a CDW state in an Ni-based MX-Chain, $[Ni_2(BPCE)X_2]X_3$ (BPCE = 1,2-bis(1,4,6,8,11-pentaazacyclotetradecane-6-yl)ethane; X = Cl, Br), was recently reported by Kitagawa *et al.*[19] This CDW state is a mixed-valence Ni(II)/Ni(III) state, and is different from those of Pd- and Pt-based MX-Chains. The Ni sites are half reduced, and thus, this system does not exhibit disproportionation. Both Ni sites were reported to be low-spin states. As there has only been one report of this type of system so far, and further studies are desired in this field. Additionally, we

have previously reported Pd- and Pt-based MX-Chains having (2*S*,3*S*)-2,3-diaminobutane-1,4-diol (dabdOH) ligands.[20–23] $[Pd(dabdOH)_2Br]Br_2$ was revealed to have the Pd(III) MH state and to exhibit the highest electrical conductivity (3–38 S cm^{-1}) among all reported MX-Chains.[20] On the other hand, $[Pt(dabdOH)_2Br]Br_2$ was revealed to have the Pt(II)/Pt(IV) CDW state and to show the smallest optical gap (1.19 eV) among the reported Pt–Br-type MX-Chains.[21] These particular structures and characteristics are afforded by the chemical pressure along the chain direction as a result of the multiply hydrogen-bonded networks between the hydroxy groups on the ligands and the counter anions. Compared to these 4d/5d-transition metal MX-Chains, the achievement of such chemical pressure in 3d-transition metal Ni MX-Chains was originally considered to be more challenging due to the shorter Ni···Ni distance.[13] Such structural mismatch may create an unusual structure and electronic state.

In this work, we synthesized the first example of an electrical conductive Ni-based MX-Chain compound with hydroxy groups by using dabdOH ligands. Interestingly, X-ray diffraction, spectroscopic, and magnetic measurements revealed that the MX-Chain adopted an intermediate state between the MH and CDW states, as well as mixed-valence high-spin Ni(II) and low-spin Ni(III). The partial deprotonation of the hydroxy groups on the ligands (represented as $dabdOH_x$, where x is the fraction of protonated –OH, x = ~0.6), together with the partial lack of counter anions, was suggested to play an important role in achieving this peculiar structure and electronic state. This intermediate electronic state is a new state of the MX-Chains, which is different from neither the conventional Ni(III) MH state, phase transition state of Pd(II)/Pd(IV) CDW to Pd(III) MH in the Pd-type MX-Chains,[24,25] nor the boundary state between Pt(III) MH and Pt(II)/Pt(IV) CDW in the Pt-type MX-Chains.[26]

Results and Discussion

Synthesis and Crystal Structures

Refluxing the starting materials $NiBr_2$ and dabdOH in MeOH afforded a blue solution (Scheme 1), indicating the in-situ generation of the bis-type Ni(II) complex with diamine ligands.[27] After electrochemical oxidation in the presence of an excess of Br^- ions, brown plate single crystals of **1**·solvent were obtained on the anode.

Figures 1 and S1 show the crystal structure of **1**·solvent. Crystallographic data and selected bond lengths are listed in Tables S1 and S2, respectively. The crystal structure contains two crystallographically independent Ni atoms. The Ni centers are coordinated by two dabdOH chelating ligands in the equatorial positions to form a bis-type complex (Figure 1a). The Br ions coordinate to the axial positions to form 1D Ni–Br chains. The bridging Br ions are located at the exact midpoint between Ni atoms, suggesting a MH-like state. The Ni···Ni distance was 5.2115(3) Å at 120 K and 5.2406(3) Å at room temperature; these values correspond to the length of the shortest axis. In addition, the Ni(1) chains have two Br counter ions per Ni complex moiety, forming a 2D-sheet structure $[Ni(dabdOH)_2Br]Br_2$ via the triple hydrogen-bonding network of NH···Br (N···Br = 3.519(8) and 3.560(8) Å) and OH···Br (O···Br = 3.266(6) Å), as shown in Figure 1b. Such 2D-sheet structures are typical among MX-chains, e.g., $[Ni(bn)_2Br]Br_2$ (bn: 2*S*,3*S*-diaminobutane),[28] $[Ni(chxn)_2Br]Br_2$,[17] and $[Pd(dabdOH)_2X]X_2$ (X = Br, Cl).[20,23]

The chains of Ni(1) and Ni(2) are parallel, and the Ni···Ni distance is crystallographically equivalent, but the coordinating orientations of ligands in two chains are perpendicular to each other. The Ni(2) chains are isolated between the sheets of Ni(1) chains and have no counter anions (Figure 1c). It is noted that the hydroxy groups of the dabdOH ligands were partially deprotonated, i.e., $[Ni(dabdOH_x)_2Br]$ ($x < 1$), which was confirmed from the IR spectra and the quantum chemical

calculations (*vide infra*). The deprotonation of the amino groups was negligible, because the Ni–N bond lengths of Ni(2) (2.072(5) Å) were not shorter than those of Ni(1) (1.990(4) and 1.994(4) Å) (Table S2). The Ni–N bond length of the amido group (1.801(3) Å) has been reported to be shorter than that of the amino group (1.945(3) Å).[29] The slight elongation of the Ni–N bonds of Ni(2) was attributed to the lack of hydrogen bonding with counter anions. In addition, **1**·solvent contained both Ni(II) and Ni(III), as revealed by magnetic measurements (*vide infra*). These measurements suggested that the fraction of protonated hydroxy groups (x) can be estimated to be ~0.6, although the exact number is uncertain. As the diffraction spot pattern featured weak spots with double periodicity along the a and b axes on the (hk0) plain (Figure 2), the crystal structure was solved as the superlattice. This superlattice indicates a structure in which single chains of Ni(2) are accompanied by adjacent pores (Figure 1c). The phase information is lost on the screen in the X-ray diffraction measurements, which is known as the phase problem.[30] Direct methods are known as a powerful tool for estimating the phases; however, the phase information is lost once on the screen. In other words, three-dimensional wave information involving phase is reduced to location and intensity as diffraction spots on the two-dimensional screen. On the other hand, phases A and B shown in Figure 1c are identical in terms of crystal structure and orientation and differ only in their phase. Structures of phases A and B are identical in crystallography; however, the locations of the Ni(2) chains and pores are replaced each other. Therefore, as a real substance, two possible structures can be considered, i.e., a single-domain structure or a multi-domain structure. The former is single-phase and is composed of the complete structure throughout the whole single crystal, i.e., the Ni(1) sheets, Ni(2) chains, and pores. In contrast, the latter is composed of two phases, i.e., phases A and B. In this multi-domain structure, the Ni(2) chains in phase A grow perpendicular to the plane of the page in the figure, and the phase changes to phase B at the boundary of the domain. The Ni(2) chains are disconnected at the boundary, forming

closed pore spaces. The rigid frameworks of the Ni(1) hydrogen-bonded sheets do not change between these phases, which is necessary for growth of a single crystal. However, single chains of Ni(2) are not rigid and can be disorder. When the domain size is enough large to afford spots rather than diffuse scattering, superlattice reflection can be observed. Therefore, even if a single crystal has a multi-domain structure containing phases A and B, the phase difference is lost on the screen, and then these are treated as identical in crystallography. Two possible structures, i.e., a single-domain structure or a multi-domain structure, cannot be distinguished in the X-ray diffraction measurements.

In addition, weak electron density derived from solvents retained in the pore spaces was detected. As these electron densities were located at special positions in the lattice, they were treated using the SQUEEZE method in the software Olex2 to facilitate solving the structure.[31] Additionally, the superlattice reflections along the c axis of the chain direction did not appear on the (0kl) and (h0l) planes (Figure S2). If **1**·solvent had a CDW state, the corresponding superlattice would be observed. MX-Chains of the CDW state can be represented as $\cdots X–M^{IV}–X\cdots M^{II}\cdots X–$ (M = Pd or Pt)[14,15] or $\cdots X–Ni^{III}–X\cdots Ni^{II}\cdots X–$.[19] The CDW state is 1:1 mixed-valence state, i.e., M^{IV}:M^{II}=1:1 or Ni^{III}:Ni^{II}=1:1. On the other hand, **1**·solvent is Ni^{III}:Ni^{II}=~85:~15 (*vide infra*), which is inclined to the Ni^{III} side. Major components would be –Br–Ni^{III}–Br–Ni^{III}–Br–, but –Br$\cdots Ni^{II}\cdots$Br– parts would be randomly contained in some places. Crystal structure would be averaged to the major component side. Since **1**·solvent is not a complete CDW state, it would not be expected to show the reflections of the CDW state. Additionally, as –Br–Ni^{III}–Br–Ni^{III}–Br– components are Raman forbidden, the signals of –Br$\cdots Ni^{II}\cdots$Br– parts can be detected even minor components (*vide infra*). Therefore, **1**·solvent is not a CDW state but an intermediate state between the MH and CDW states.

If closed pore spaces were present in the crystal, solvent molecules could be trapped in these spaces. The ^{1}H NMR spectrum of **1**·solvent in D_2O contains almost equal amounts of 2-PrOH

and MeOH (Figure S3). Elemental analyses revealed that **1**·solvent retained these solvent molecules after drying in vacuo at room temperature (Figure 3). Moreover, these solvent molecules were not evacuated after drying in vacuo at 373 K overnight. Additionally, TG-DTA of **1**·solvent indicated a small weight loss (–4.8 wt%) at 435 K under an N_2 atmosphere (Figure S4). A similar small weight loss has been reported in MX-Chains with the dabdOH ligands, i.e., $[Pd(dabdOH)_2Br]Br_2$[20] and $[Pd(dabdOH)_2Cl]Cl_2$,[23] at same temperature region. These MX-Chain compounds have no solvent molecule. Therefore, the small weight loss of **1**·solvent can be decomposition of the dabdOH ligands rather than evacuation of solvent molecules. The solvent molecules would be evacuated during the subsequent decomposition processes. The ^{1}H NMR and elemental analyses strongly support the existence of trapped solvent molecules in the pore spaces. However, the single-domain structure can also be considered, as the solvent molecules could be caught in the constricted pores (Figure 1d).

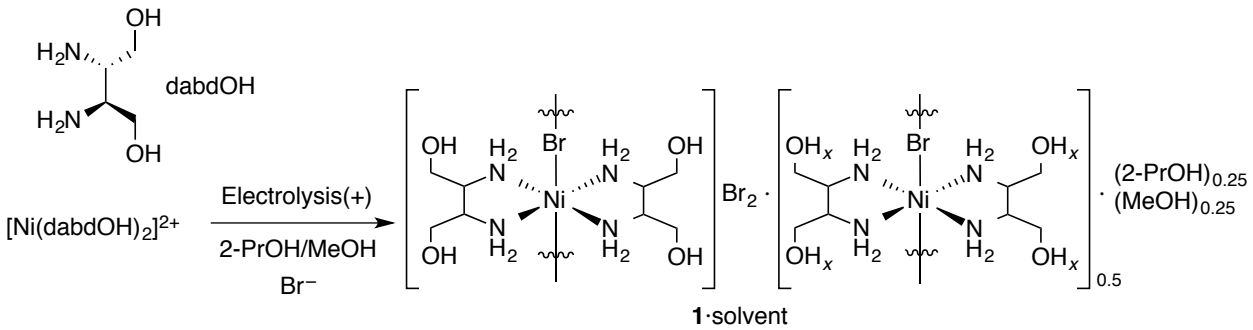

Scheme 1. Synthetic scheme of **1**·solvent.

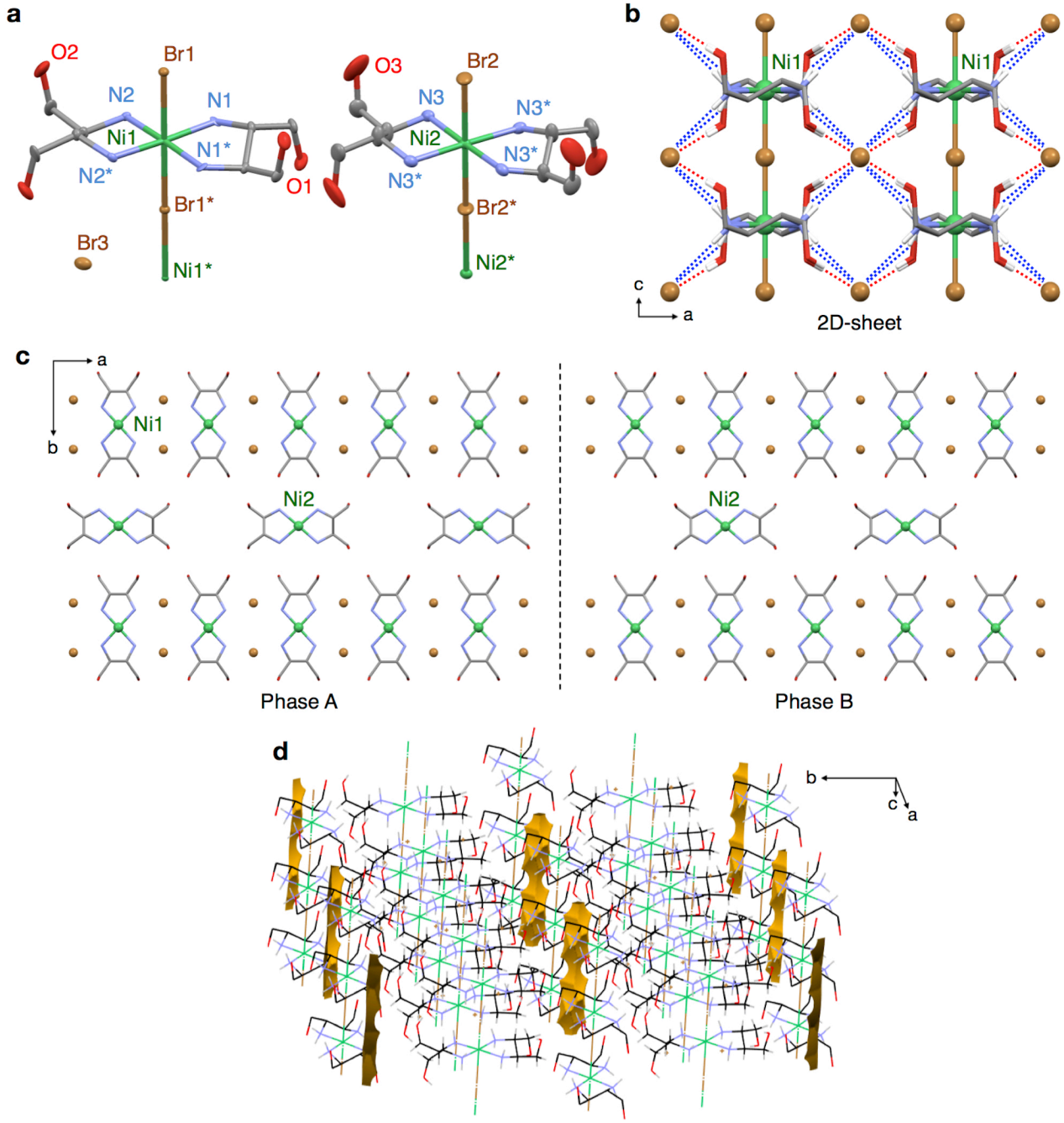

Figure 1. Crystal structure of **1**·solvent. (a) Molecular structures with atomic displacement parameters at 50% probability. (b) Hydrogen bonding network of OH···Br (red dotted lines) and NH···Br (blue dotted lines). (c) Packing structures as phases A and B shown as ball-and-stick models. Color code: Ni = green, Br = yellow, N = light blue, O = red, C = grey, and H = white. Selected hydrogen atoms have been omitted for clarity, and only selected atoms are labeled. (d) Solvent-accessible void space (yellow) occupied by solvent molecules calculated by Mercury[32] using a probe radius of 1.8 Å (MeOH) and grid spacing of 0.1 Å. The contact surface void volume is ca. 206 Å^3 (7.6% of the unit cell volume), which was calculated using the same probe radius and grid spacing.

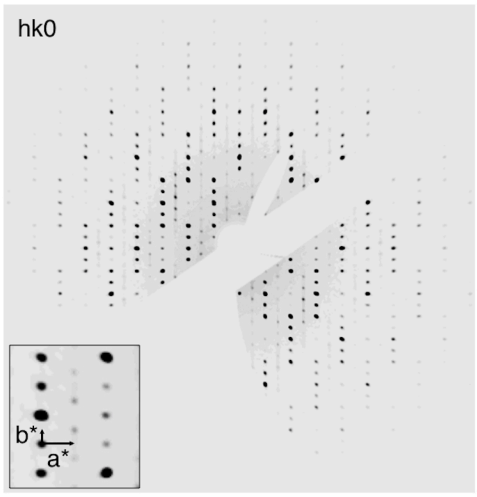

Figure 2. Single-crystal X-ray diffraction spot pattern on the (hk0) plain for **1**·solvent.

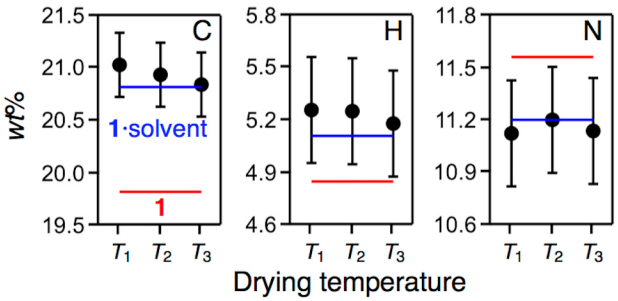

Figure 3. Plots of the elemental analysis data (C, H, N) for **1**·solvent after being dried in vacuo for 12 h at r.t. (T_1), 333 K (T_2), and 373 K (T_3), together with the experimental error bars (0.3%). The horizontal lines represent the calculated elemental wt% for the compositions $[Ni(dabdOH)_2Br]Br_2 \cdot [Ni(dabdOH_x)_2Br]_{0.5} \cdot (2\text{-PrOH})_{0.25} \cdot (MeOH)_{0.25}$ (**1**·solvent, blue lines) and $[Ni(dabdOH)_2Br]Br_2 \cdot [Ni(dabdOH_x)_2Br]_{0.5}$ (**1**, red lines) with $x = 0.5$.

Spectral and Conductive Properties

Figure 4a shows the polarized reflection spectra for a single crystal of **1**·solvent. The spectrum measured from an electric vector parallel to the chain showed a relatively high intensity band at around 0.8 eV after the Kramers–Kronig transform. This band can be assigned as a charge-transfer (CT) transition from the occupied Br band to the empty d_z^2 band or the upper-Hubbard band of the chains.[28,33] In contrast, this CT band disappeared entirely in the spectrum measured from a perpendicular electric vector. This anisotropy strongly indicates the 1D electronic structure of the single crystal of **1**·solvent. In comparison, previously reported Ni-based MX-Chains showed CT bands at 1.3 eV ($[Ni(chxn)_2Br]Br_2$ and $[Ni(bn)_2Br]Br_2$)[28] and 1.5 eV ($[Ni(chxn)_2Br](NO_3)_2$).[33] In comparison with these absorption bands, that of **1**·solvent (0.8 eV) appeared at lower energy. It was reported that the CDW state of $[Pd(chxn)_2Br]Br_2$ showed an absorption band at 0.75 eV derived from the transition from the Pd(II) d_z^2 band to the Pd(IV) d_z^2 band.[34] In the CDW state, the absorption energy has been revealed to decrease with decreasing difference between the M(II)–X and M(IV)···X bond lengths.[35] In the case of **1**·solvent, the Ni–Br bond lengths were crystallographically equivalent, i.e., any small difference between them could not be distinguished using X-ray diffraction (Figure 1), even if **1**·solvent contains CDW components. Therefore, **1**·solvent may exhibit a modulated Ni(III) MH state rather than an absolute one; an intermediate state between the MH and the CDW states can be considered. The polarized Raman spectrum for a single crystal of **1**·solvent showed a peak at 145 cm^{-1} (Figure 4b). This peak can be assigned as a symmetric stretching mode of Br–Ni–Br, which is a forbidden mode in the MH state.[20–23,36,37] Thus, **1**·solvent appeared to be in a MH-like state based on X-ray diffraction; however, it also contained a CDW-like state, as revealed by these spectra.

Figure 5 shows the IR spectra for simulated $[Ni^{II}(dabdOH)_2]^{2+}$ and $[Ni^{III}(dabdOH)_2Br_2]^{+}$ obtained using density functional theory (DFT) calculations (Figure 6 and Tables S3–S6),[38,39]

polycrystals of $[Pd(dabdOH)_2]Br_2$, polycrystals of **1**·solvent, and a single crystal of **1**·solvent obtained from the polarized reflection IR spectra after the Kramers–Kronig transform, respectively. Polycrystals of $[Pd(dabdOH)_2]Br_2$, which adopts a square planar geometry (Figure S5), showed four peaks at 953, 1011, 1055, and 1092 cm^{-1}. These peaks were assigned as vibration modes, including C–O and C–N stretching (i), C–O and C–C (CH–CH_2) stretching (ii), C–C (CH–CH) stretching (iii), and O–H bending (iv) via comparison with the results of DFT calculations for square planar $[Ni^{II}(dabdOH)_2]^{2+}$ optimized at the B3LYP/LanL2DZ level of theory (Figure 5). Additionally, polycrystals of **1**·solvent showed four corresponding peaks at 949, 1009, 1058, and 1090 cm^{-1}; furthermore, an additional peak appeared at 1033 cm^{-1}. Measurement of a single crystal of **1**·solvent using a polarizer separated the C–O and C–C stretching vibration modes of the dabdOH ligands, as the direction of the C–O bond is nearly parallel to the chain direction and nearly perpendicular to the ligand plane. As the directions of the C–N bonds include vertical components toward the reflection plane (a–c plane), the intensity of the C–N stretching would become weak. The spectrum parallel to the chain direction showed peaks at 949, 1015, and 1092 cm^{-1}, which were assigned as the C–O stretching derived from (i), the C–O stretching derived from (ii), and the O–H bending derived from (iv), respectively. The parallel spectrum also showed an additional peak at 1033 cm^{-1}, which was assigned as C–O stretching because of the parallel component. This additional C–O stretching can be considered to be derived from the vibration modes of #52 and/or #53 for $[Ni^{II}(dabdOH)_2]^{2+}$ and #55 and/or #58 for $[Ni^{III}(dabdOH)_2Br_2]^{+}$ (Figure 6). These vibration modes are originally forbidden or weak in intensity, as the dipole moment is almost unchanged. However, partial deprotonation of the hydroxy group, i.e., of the $dabdOH_x$ ligands, would afford asymmetric –OH and $–O^{–}$ moieties, increasing the intensity of the vibration modes of #52 and/or #53 for $[Ni^{II}(dabdOH)_2]^{2+}$ and #55 and/or #58 for $[Ni^{III}(dabdOH)_2Br_2]^{+}$. Therefore, the additional peak was assigned as C–O stretching of the

deprotonated form, which provides evidence of the partial deprotonation of the hydroxy groups on the dabdOH ligands in **1**·solvent. It is noteworthy that both polycrystals of **1**·solvent and a single crystal of **1**·solvent showed this additional peak, as this clearly refutes the concern that **1**·solvent is a mixture of crystals with a protonated form and a deprotonated form.

In addition, the electrical conductivity for a single crystal of **1**·solvent was measured using the two-point probe method (Figure 7a). The probes were attached at opposite sides of the chain direction using carbon paste.[40] The conductivity of **1**·solvent at 300 K (σ_{300K} = 3.1±2.1 × 10^{-4} S cm^{-1}) was estimated using the crystal size and the differential resistance at 0 V to avoid the Joule heating effect (Figure S6) and was measured using several single crystals. The conductivity decreased with decreasing temperature, indicating a semiconductor characteristic. The Arrhenius plot afforded an activation energy (E_a) of 233±4 meV. In comparison to the previously reported bromide-bridged MX-Chains, i.e., $[Ni(bn)_2Br]Br_2$,[28] $[Ni(chxn)_2Br]Br_2$,[40] and $[Ni(chxn)_2Br](NO_3)_2$ (Figure S7), **1**·solvent had lower conductivity (Figure 7b). The log-scale conductivity shows a roughly negative correlation with the Ni···Ni distance of the chain; thus, one reason for the low conductivity for **1**·solvent is its longer Ni···Ni distance. The elongation of the Ni···Ni distance weakens the orbital overlap between d_z^2 and p_z. Furthermore, mixing of the CDW-like state with the MH state may also favor insulation.

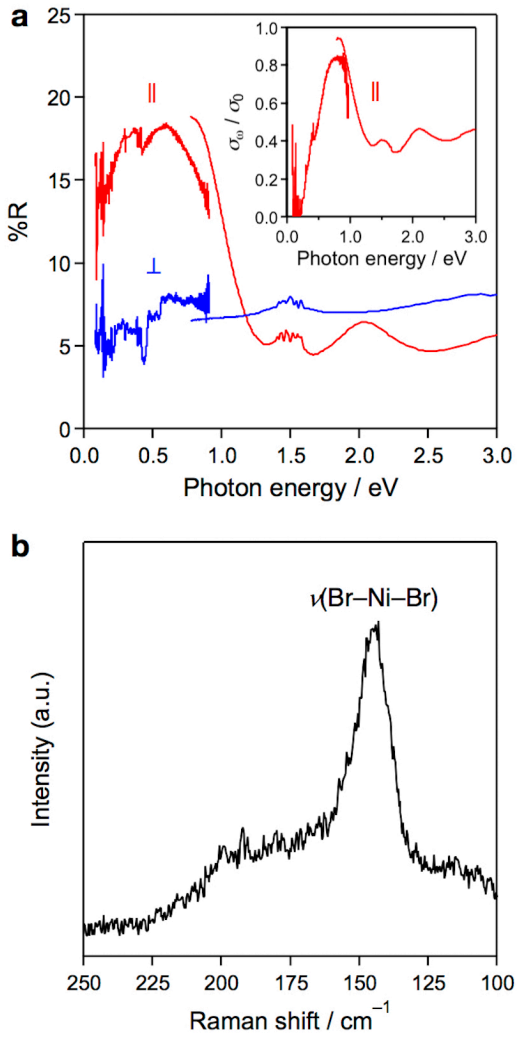

Figure 4. (a) Polarized reflection spectra parallel (∥: red line) and perpendicular (⊥: blue line) to the chain direction of a single crystal of **1**·solvent. Inset shows an optical conductivity spectrum parallel after the Kramers–Kronig transform. (b) Polarized Raman spectrum parallel to the chain direction of a single crystal of **1**·solvent.

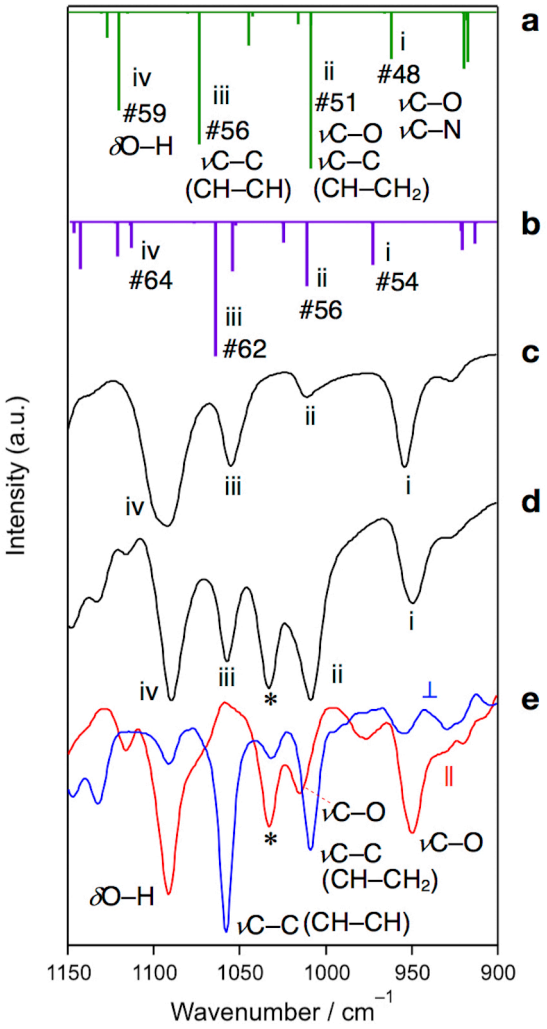

Figure 5. IR spectra of (a) simulated $[Ni^{II}(dabdOH)_2]^{2+}$ (B3LYP/LanL2DZ) and (b) simulated $[Ni^{III}(dabdOH)_2Br_2]^{+}$ (UB3LYP/LanL2DZ), (c) polycrystals of $[Pd(dabdOH)_2]Br_2$ (KBr), (d) polycrystals of **1**·solvent (KBr), and (e) a single crystal of **1**·solvent using a polarizer (∥: red line; ⊥: blue line) after the Kramers–Kronig transform. The peaks marked with an asterisk (*) can be assigned as νC–O of a deprotonated form.

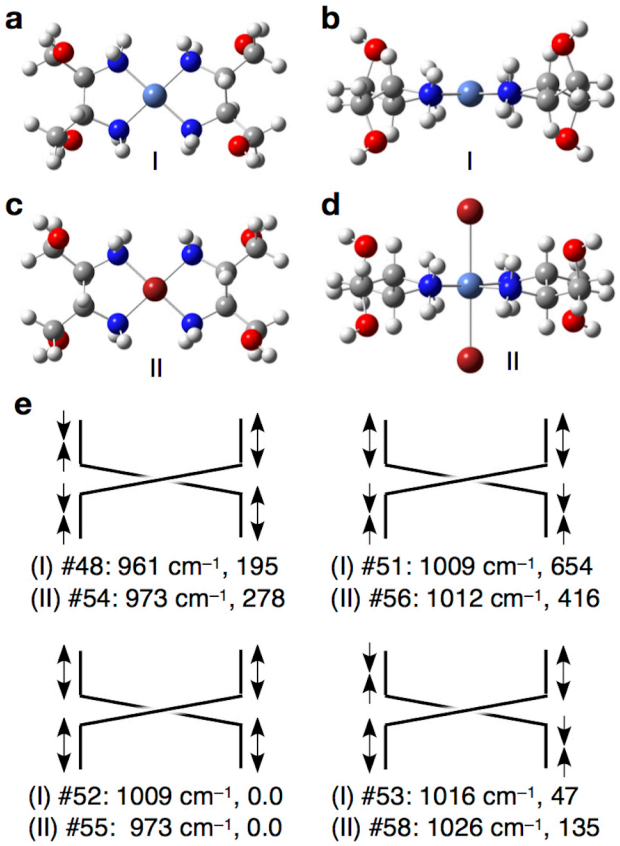

Figure 6. (a) Top view and (b) side view of the optimized structure of $[Ni^{II}(dabdOH)_2]^{2+}$ (I) obtained using B3LYP/LanL2DZ and (c, d) those of $[Ni^{III}(dabdOH)_2]^{+}$ (II) obtained using UB3LYP/LanL2DZ. (e) Diagrams of the vibration modes including C–O stretching, along with the calculated energy and intensity.

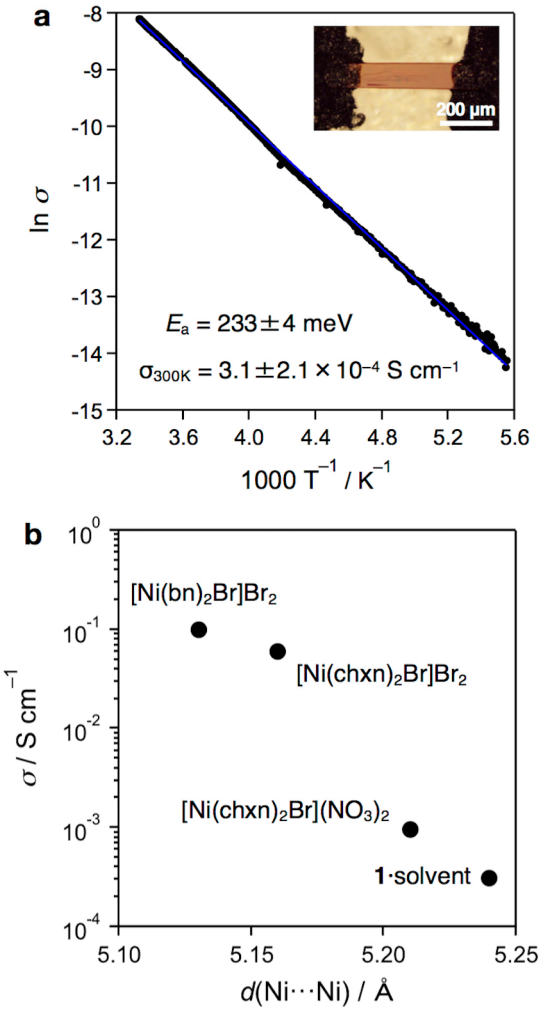

Figure 7. (a) Arrhenius plot of the electrical conductivity of a single crystal of **1**·solvent measured at a 0.2 V bias. The inset photograph shows a micro-photo-image of **1**·solvent after the attachment of the probes using carbon paste in the side-attachment configuration. (b) Comparison of the electrical conductivity at 300 K for $[Ni(bn)_2Br]Br_2$,[28] $[Ni(chxn)_2Br]Br_2$,[17,40] $[Ni(chxn)_2Br](NO_3)_2$ (Figure S7),[33] and **1**·solvent vs the Ni···Ni distances. The Ni···Ni distance for $[Ni(bn)_2Br]Br_2$ was measured at 121 K, whereas the others were measured at 296 K.

Magnetic Properties

Ni-based MX-Chain compounds have been reported to exhibit strong antiferromagnetism between the low-spin Ni(III) (S = 1/2) sites on the chain, in accordance with the Bonner–Fisher model for a Heisenberg-type antiferromagnet.[17,28,33] Their exchange interactions (J) were reported to be approximately –1000 to –3000 K, indicating that the chains showed negligible magnetization near room temperature. On the other hand, **1**·solvent exhibited weak antiferromagnetism (Figures 8 and S8). The $\chi_m T$ value increased to 0.46 cm^3 K mol_{Ni}^{-1} at approximately 380 K, which significantly exceeds the $\chi_m T$ value for the spin-only case with S = 1/2 (0.375 cm^3 K mol^{-1}). This weak antiferromagnetism is abnormal among the Ni-based MX-Chains.[17,28,33] Additionally, the previously reported Ni(III) MH state of $[Ni(en)_2Br](ClO_4)_2$ (en: ethylenediamine) had a longer Ni···Ni distance (5.28 Å) than **1**·solvent (5.24 Å) but showed stronger antiferromagnetism (J = ca. –1700 K).[41] The large $\chi_m T$ value for **1**·solvent cannot be explained without the existence of high-spin Ni(II) (S = 1). Hence, mixed-valence Ni(II) and Ni(III) sites with an intermediate state between the MH and CDW states were considered for **1**·solvent. As the spin-only $\chi_m T$ value for pure Ni(II) is 1.0, the ratio of Ni(II) in **1**·solvent was estimated to be at least ~15%. The Ni(II) site should be in a high-spin state, because the Ni–Br bond length (2.62 Å at 300 K) is sufficiently short and comparable to those of reported high-spin Ni(II) sites, e.g., $[Ni_2(L)Br_2](ClO_4)_2$ (L = *α,α′*-bis-{(5,7-dimethyl-1,4,8,11-tetraazacyclotetradeca-6-yl)-*o*-xylene}; Ni(II)–Br = 2.62 and 2.71 Å).[42] In contrast, the bond length for low-spin Ni(II)–Br is longer, and has been reported to be 2.88–3.32 Å,[42] with values of 2.98 and 3.04 Å in the Ni(II)/Ni(III) CDW state of the MX-Chain $[Ni_2(BPCE)Br_2]Br_3$.[19] On the other hand, the Ni(III)–Br bond lengths of the low-spin states were reported to be 2.58 Å in $[Ni(chxn)_2Br]Br_2$[17] and 2.63 and 2.67 Å in $[Ni_2(BPCE)Br_2]Br_3$.[19] The Ni–Br bond length (2.62 Å) in **1**·solvent falls within

this range, indicating low-spin Ni(III) sites. The crystallographically obtained Ni–Br bond length is thus consistent with both high-spin Ni(II) and low-spin Ni(III) states.

The strong antiferromagnetism (ca. –1000 K) is generally found in Mott insulators.[43] In the case of MX-Chains, superexchange interactions between d_z^2 and p_z orbitals can also contribute antiferromagnetism. It is represented as –↑–↓↑–↓–↑↓–↑– in the Ni(III) MH state. On the other hand, the reported Ni(II)/Ni(III) MX-Chain compound $[Ni_2(BPCE)Br_2]Br_3$ with both low-spin states shows a weak antiferromagnetism (J = –178 K) which can be represented as –↑–↓↑–↓↑–↓↑–↓–.[19] Therefore, being the MH state is critical for the strong antiferromagnetism of MX-Chains. Superexchange interactions would be only a minor impact. As **1**·solvent is not the MH state but an intermediate state between the MH and CDW states, the strong antiferromagnetism characterized in Mott insulator would not express.

Figure 9 shows the ESR spectra of polycrystals of **1**·solvent at various temperatures. The main signal appeared at ~3140 G at each temperature, indicating a g value of 2.184. This main signal was assigned as a permitted transition with $\Delta M_S = \pm 1$ derived from the S = 1/2 low-spin Ni(III) sites. On the other hand, at around ~1500 G, a weak signal with g = 4.157 appeared. This weak signal was assigned as a forbidden transition with $\Delta M_S = \pm 2$ derived from the high-spin Ni(II) (S = 1) sites. This forbidden transition was considered to be the half-field transition of the triplet system,[44–46] which strongly indicates the existence of high-spin Ni(II). This is the first evidence for high-spin Ni(II) in Ni-based MX-Chains. The peak-to-peak line width (ΔH_{pp}) was 85 G at 4 K, whereas that at 150 K was broadened to 127 G. Above 150 K, the signal was extremely broadened and difficult to detect. This broadening has been reported to be a common property of the MH state of MX-Chains.[20,23,34,47] Therefore, the magnetic properties exhibited both mixed-valence and MH-like nature, indicating the coexistence of the MH-like state and the mixed-valence state.

The mixed-valence state of the Ni-based MX-Chain of **1**·solvent is different from the mixed-valence states of Pd- and Pt-based MX-Chains, since the former has II/III mixed valency, while the latter have II/IV mixed valency. Figure 10 shows a plot of the Ni(II)/Ni(III) ratio and the Ni···Ni distance in the bromide-bridged Ni-based MX-Chains. A longer Ni···Ni distance tends to afford the CDW state, while a shorter distance tends to afford the MH state. The behavior of **1**·solvent is exceptional, since it would be expected to exhibit the MH state based on its Ni···Ni distance. The partial lack of counter anions for Ni(2) chains could be a reason for the occurrence of the intermediate state, as the typical chemical formula of MX-Chains is $[M(A)_2X]Y_2$. If all hydroxy groups on the ligands were protonated, i.e., x = 1 in $[Ni(dabdOH_x)_2Br]$ for Ni(2), **1**·solvent would have a Ni(II)/Ni(III) ratio of 2/1 based on the charge valance. If the x value were 0.5, the all-Ni(III) MH state would be afforded. However, as the magnetic measurements suggested that Ni(II)/Ni(III) was at least ~0.18, x should be approximately ~0.6. The Ni(II) sites may be randomly distributed in the Ni(1) and Ni(2) chains, as the Ni–Br bond lengths are crystallographically equivalent (Figure 1). Additionally, the CT band (0.8 eV) also suggests a random distribution (Figure 4a). If the Ni(II) sites were localized in the $[Ni(dabdOH_x)_2Br]$ chains, a CT band derived from the Ni(III) sites in the $[Ni(dabdOH)_2Br]Br_2$ chains would appear at ca. 1.3–1.5 eV; however, this CT band was not observed. Although they could not be distinguished in the X-ray diffraction measurements, the positions of the bridging Br ions at the Ni(II) sites should be slightly shifted from the midpoints of Ni···Ni, since the symmetric stretching mode of Br–Ni–Br was permitted in the Raman spectrum (Figure 4b). It is noted that the previously reported $[Ni_2(BPCE)X_2]X_3$ (X = Cl, Br) adopts a ghost-leg sheet structure and can be classified as an extrema state of the Ni(II)/Ni(III) CDW.[19] In contrast, **1**·solvent forms a multi-hydrogen-bond sheet structure as well as partially deprotonated single chains. The intermediate state of **1**·solvent between MH and CDW involves a high-spin Ni(II) and a low-spin Ni(III) state, which is

quite different from the case of $[Ni_2(BPCE)X_2]X_3$, in which the Ni(II)/Ni(III) states are both low-spin. In addition, the previously reported $[Pt(chxn)_2I]I_2$ is the boundary between the Pt(III) MH and Pt(II)/Pt(IV) CDW states,[26] and is not a reduced state like those of **1**·solvent and $[Ni_2(BPCE)X_2]X_3$.

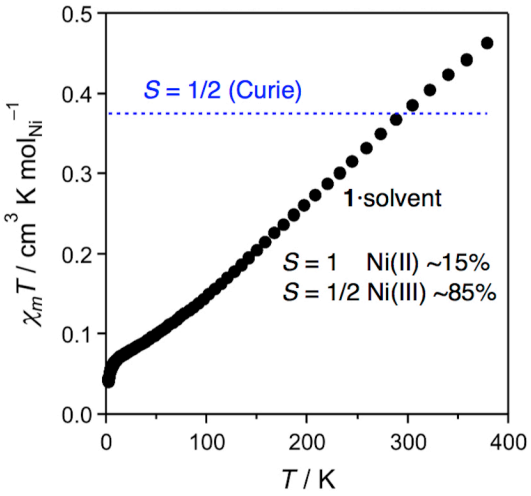

Figure 8. $\chi_m T$–T plot of polycrystals of **1**·solvent (black circles) measured under 1000 Oe.

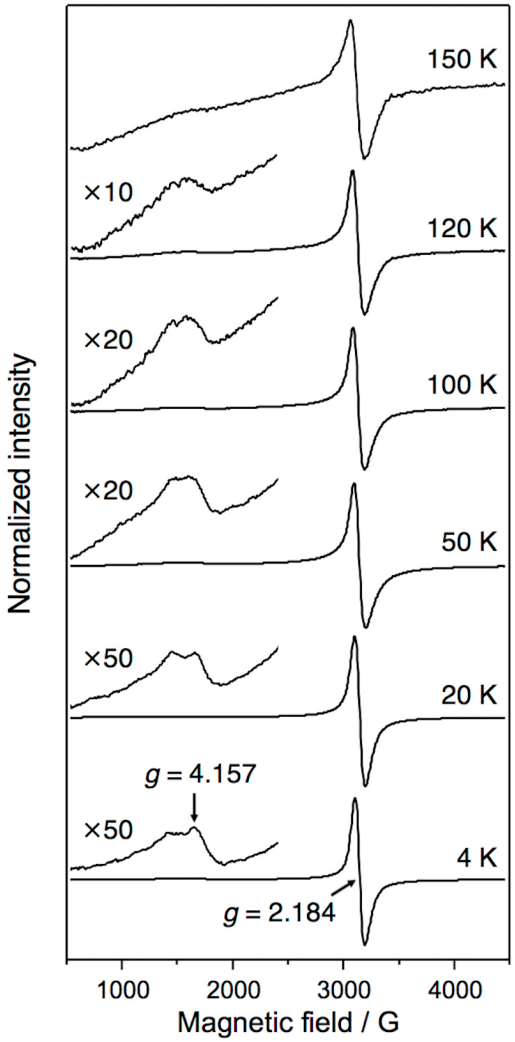

Figure 9. First-derivative ESR spectra of **1**·solvent measured at various temperatures. Insets show magnifications of the 500–2500 G region. The signals could not be measured at temperatures above 150 K due to the extreme broadening.

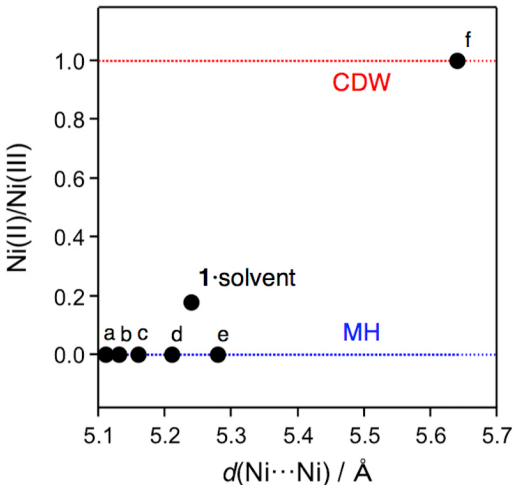

Figure 10. Plot of the Ni(II)/Ni(III) ratio and the Ni···Ni distance in **1**·solvent and other Ni-based MX-Chains. (a) $[Ni(pn)_2Br]Br_2$ (pn: (*R*)-1,2-diaminopropane),[48] (b) $[Ni(bn)_2Br]Br_2$,[28] (c) $[Ni(chxn)_2Br]Br_2$,[17] (d) $[Ni(chxn)_2Br](NO_3)_2$,[33] (e) $[Ni(en)_2Br](ClO_4)_2$,[41] and (f) $[Ni_2(BPCE)Br_2]Br_3$.[19]

Conclusions

This work demonstrated an intermediate state between the Mott–Hubbard and charge-density-wave states in an Ni-based MX-Chain for the first time. The novel Ni-based MX-Chain, **1**·solvent, formed sheet and single-chain structures in the superlattice and performed as a semiconductor. The Ni sites were mixed-valence, with high-spin Ni(II) and low-spin Ni(III) sites. This finding represents a new structural and electronic state of one-dimensional electronic systems.

Methods

Materials. $NiBr_2$, methanol (MeOH), and 2-propanol (2-PrOH) were purchased from Fujifilm Wako Pure Chemical Corp. *n*-Tetrabutylammonium bromide ($[nBu_4N]Br$), *n*-tetrabutylammonium nitrate ($[nBu_4N]NO_3$), and 1*R*,2*R*-diaminocyclohexane (chxn) were purchased from Sigma-Aldrich. The dabdOH was prepared according to previously reported procedures.[20] Single crystals of $[Ni(chxn)_2Br](NO_3)_2$ were prepared via electrochemical oxidation at 40 μA for 3–4 days in MeOH

with [nBu$_4$N]NO$_3$ according to previously reported procedures.[33]

Synthesis of [Ni(dabdOH)$_2$Br]Br$_2$·[Ni(dabdOH$_x$)$_2$Br]$_{0.5}$·(2-PrOH)$_{0.25}$·(MeOH)$_{0.25}$ (1·solvent). Refluxing dabdOH (200 mg, 1.66 mmol) and NiBr$_2$ (218 mg, 1.00 mmol) in MeOH (27 mL) for 1 h afforded a blue solution. After the solution was cooled to room temperature, a 1.5 mL batch of the solution was transferred into a 20 mL vial. 2-PrOH (3.0 mL) and [nBu$_4$N]Br (170 mg, 0.12 M) were added as an electrolyte, and the solution was then electrolyzed at 10 μA for 1–2 days with Pt electrodes (ϕ 0.3 mm) under the ambient atmosphere and temperature using a direct current multisource system (YAZAWA CS-12Z). The electrodes were submerged 4–5 mm into the solution. Brown platelet single crystals were generated on the anode. After rinsing the electrodes with 2-PrOH and removing the crystals from the anode, the crystals were immediately dried in vacuo overnight. Crystals of **1**·solvent were obtained in ~40% yield per batch. These crystals were unstable under high-humidity conditions, but could be handled under a relatively dry air atmosphere with no difficulty. Elemental analysis calcd (%) for C$_{13}$H$_{38}$N$_6$Br$_{3.5}$Ni$_{1.5}$O$_{6.5}$ (**1**·solvent, x = 0.5): C 20.81, H 5.11, N 11.20, Br 37.28; for C$_{13}$H$_{38.2}$N$_6$Br$_{3.5}$Ni$_{1.5}$O$_{6.5}$ (**1**·solvent, x = 0.6): C 20.81, H 5.13, N 11.20, Br 37.27; found: C 21.03, H 5.26, N 11.12, Br 37.09.

Measurements. The elemental analyses were performed by using J-Science Lab Co. Ltd. JM11 and Yanaco YHS-11 at the Research and Analytical Center for Giant Molecules (Tohoku Univ.). The polarized reflection spectra and Raman spectra were measured on a JASCO MSV-5300YMT (UV-Vis-NIR) and IRT-7200 (IR) spectrometers and a HORIBA LabRAM HR-800 with He–Ne laser (633 nm) at ambient temperature and pressure in micro spectroscopy using a single crystal of the sample. The IR spectra of polycrystal samples were measured by JASCO FT/IR-4200 spectrometer using KBr

plates. The electrical conducting measurements were recorded in the liquid He cryostat of a Quantum Design PPMS (Physical Property Measuring System) MODEL 6000 using a two-contact probe method with Au wires (ϕ = 50 μm). The wires were attached using carbon paste (Dotite XC-12). Magnetic measurements were performed using a magnetic property measurement system (MPMS3, Quantum Design) in direct current mode. The sample was filled into a thermally stable plastic tube which was fixed in a brass straw for measurements below 400 K. Electron spin resonance (ESR) spectra were measured at X-band (9.608 GHz) using a Bruker E-500 spectrometer equipped with a gas-flow type cryostat Oxford ESR 900. Thermogravimetry-differential thermal analysis (TG-DTA) was performed on a Shimadzu DTG-60H.

Collection of crystallographic data and structure refinements. Suitable single crystals of **1**·solvent and $[Pd(dabdOH)_2]Br_2$ were selected and mounted onto a MicroMount (MiTeGen) in an XtaLAB AFC10 diffractometer with a HyPix-6000HE hybrid pixel array detector. The crystal was kept at 296 or 120 K using a N_2 flow-type temperature controller during data collection. Using Olex2,[31a] the structure was solved with the SHELXT[31b] structure solution program using intrinsic phasing, and refined with the SHELXL[31c] refinement package using least-squares minimization. A summary of the crystallographic data for **1**·solvent and $[Pd(dabdOH)_2]Br_2$ is shown in Table S1. The X-ray crystallographic coordinates used for the structure determination reported in this article have been deposited at the Cambridge Crystallographic Data Centre (CCDC) under deposition numbers CCDC-2105069 (**1**·solvent at 120 K) and -2132517 ($[Pd(dabdOH)_2]Br_2$ at 120 K). The data can be obtained free of charge from The Cambridge Crystallographic Data Centre via www.ccdc.cam.ac.uk/data_request/cif.

Quantum chemical calculations. Geometry optimization and frequency for $[Ni^{II}(dabdOH)_2]^{2+}$ and $[Ni^{III}(dabdOH)_2Br_2]^{+}$ in the electronic ground state were carried out in DFT B3LYP/LanL2DZ and UB3LYP/LanL2DZ, respectively. The spin multiplicities were set to singlet and doublet, respectively. All calculations were performed using the Gaussian 16W package.[38] The optimized structure, the Cartesian coordinates, and the vibration energies are given in Figure 6 and Tables S3–S6. The vibration energies were calibrated using the reported scaling factor (0.961).[39]

Supporting information. Crystal structure and crystallographic data, X-ray diffraction images, ^{1}H NMR, TG-DTA, quantum chemical calculation data, *I–V* curves, Magnetic susceptibility. (PDF)

Acknowledgement. This work was supported by a JSPS KAKENHI Grant nos. 19H05631 and 21H01756 as well as the Murata Science Foundation (M21-126). M.Y. thanks the 111 project (B18030) from China.

Conflicts of interest. There are no conflicts to declare.

Contributions. M.W. and M.R.M. are equal contribution.

References

(1) Kobayashi, H.; Kobayashi, A.; Cassoux, P. BETS as a source of molecular magnetic superconductors (BETS = bis(ethylenedithio)tetraselenafulvalene), *Chem. Soc. Rev.* **2000**, *29*, 325–333.

(2) Enoki, T.; Miyazaki, A. Magnetic TTF-based charge-transfer complexes, *Chem. Rev*. **2004**, *104*, 5449–5477.

(3) Cassoux, P.; Valade, L.; Kobayashi, H.; Kobayashi, A.; Clark, R. A.; Underhill, A. E. Molecular metals and superconductors derived from metal complexes of 1,3-dithiol-2-thione-4,5-dithiolate (dmit), *Coord. Chem. Rev*. **1991**, *110*, 115–160.

(4) Robertson, N.; Cronin, L. Metal bis-1,2-dithiolene complexes in conducting or magnetic crystalline assemblies, *Coord. Chem. Rev*. **2002**, *227*, 93–127.

(5) Bockrath, M.; Cobden, D. H.; Lu, J.; Rinzler, A. G.; Smalley, R. E.; Balents, L.; McEuen, P. L. Luttinger-liquid behaviour in carbon nanotubes, *Nature* **1999**, 397, 598–601.

(6) Yao, Z.; Postma, H. W. Ch.; Balents, L.; Dekker, C. Carbon nanotube intramolecular junctions, *Nature* **1999**, *402*, 273–276.

(7) Ishii, H.; Kataura, H.; Shiozawa, H.; Yoshioka, H.; Otsubo, H.; Takayama, Y.; Miyahara, T.; Suzuki, S.; Achiba, Y.; Nakatake, M.; Narimura, T.; Higashiguchi, M.; Shimada, K.; Namatame, H.; Taniguchi, M. Direct observation of Tomonaga–Luttinger-liquid state in carbon nanotubes at low temperatures, *Nature* **2003**, *426*, 540–544.

(8) Givaja, G.; Amo-Ochoa, P.; Gómez-García, C. J.; Zamora, F. Electrical conductive coordination polymers, *Chem. Soc. Rev.* **2012**, *41*, 115–147.

(9) Voit, J. One-dimensional fermi liquids, *Rep. Prog. Phys.* **1994**, *57*, 977–1116.

(10) Seo, H.; Hotta, C.; Fukuyama, H. Toward systematic understanding of diversity of electronic properties in low-dimensional molecular solids, *Chem. Rev.* **2004**, *104*, 5005–5036.

(11) Blundell, S. J.; Pratt, F. L. Organic and molecular magnets, *J. Phys. Condens. Matter*. **2004**, *16*, R771–R828.

(12) Horiuchi, S.; Tokura, Y. Organic ferroelectrics, *Nat. Mater.* **2008**, *7*, 357–366.

(13) Yamashita, M. Next generation multifunctional nano-science on advanced metal complexes with quantum effect and nonlinearity, *Bull. Chem. Soc. Jpn*. **2021**, *94*, 209–264.

(14) Peder, L. K.; Hans, T. The crystal structure of trans-dichlorobis[(–)-1(*R*),2(*R*)-cyclohexanediamine]platinum(IV)-bis[(–)-1(*R*),2(*R*)-cyclohexanediamine]platinum(II) tetrachloride. a note on the corresponding bromide compound, *Acta Chem. Scand.* **1977**, *31A*, 182–186.

(15) Matsumoto, N.; Yamashita, M.; Kida, S. Studies on mixed valence complexes of platinum and palladium. i. preparation and characterization of Pt(II)–Pt(IV), Pd(II)–Pt(IV), and Pd(II)–Pd(IV) complexes of the general formula, $[M(AA)_2][M'X_2(AA)_2]Y_4$, *Bull. Chem. Soc. Jpn*. **1978**, *51*, 2334–2337.

(16) Yamashita, M.; Takaishi, S. Stabilization of Pd(III) states in nano-wire coordination complexes, *Chem. Commun.* **2010**, *46*, 4438–4448.

(17) Toriumi, K.; Wada, Y.; Mitani, T.; Bandow, S.; Yamashita, M.; Fujii, Y. Synthesis and crystal structure of a novel one-dimensional halogen-bridged nickel(III)-X-nickel(III) compound, {[Ni(*R*,*R*-chxn)$_2$Br]Br$_2$}.infin., *J. Am. Chem. Soc.* **1989**, *111*, 2341–2342.

(18) Nasu, K. Extended Peierls-Hubbard model for one-dimensional n-sites n-electrons system. i. phase diagram by mean field theory, *J. Phys. Soc. Jpn.* **1983**, *52*, 3865–3873.

(19) Hashiguchi, R.; Otsubo, K.; Maesato, M.; Sugimoto, K.; Fujiwara, A.; Kitagawa, H. Mixed-valence nickel bis(azamacrocycle) compounds with ghost-leg-type sheets, *Angew. Chem. Int. Ed.* **2017**, *56*, 3838–3841.

(20) Mian, M. R.; Iguchi, H.; Takaishi, S.; Murasugi, H.; Miyamoto, T.; Okamoto, H.; Tanaka, H.; Kuroda, S.; Breedlove, B. K.; Yamashita, M. Multiple-hydrogen-bond approach to uncommon Pd(III) oxidation state: a Pd–Br chain with high conductivity and thermal stability, *J. Am. Chem. Soc*. **2017**, *139*, 6562–6565.

(21) Mian, M. R.; Iguchi, H.; Takaishi, S.; Afrin, U.; Miyamoto, T.; Okamoto, H.; Yamashita, M. Smallest optical gap for Pt(II)–Pt(IV) mixed-valence Pt–Cl and Pt–Br chain complexes achieved by

using a multiple-hydrogen-bond approach, *Inorg. Chem*. **2019**, *58*, 114–120.

(22) Mian, M. R.; Afrin, U.; Iguchi, H.; Takaishi, S.; Yoshida, T.; Miyamoto, T.; Okamoto, H.; Tanaka, H.; Kuroda, S.; Yamashita, M. Conductive zigzag Pd(III)–Br chain complex realized by a multiple-hydrogen-bond approach, *CrystEngComm*, **2020**, *22*, 3999–4004.

(23) Mian, M. R.; Wakizaka, M.; Yoshida, T.; Iguchi, H.; Takaishi, S.; Afrin, U.; Miyamoto, T.; Okamoto, H.; Tanaka, H.; Kuroda, S.; Breedlove B. K.; Yamashita, M. An unusual Pd(III) oxidation state in the Pd–Cl chain complex with high thermal stability and electrical conductivity, *Dalton Trans.* **2021**, *50*, 1614–1619.

(24) Takaishi, S. Exploration of boundary between charge-density-wave and mott-hubbard states in quasi-one-dimensional halogen-bridged metal complexes, *Bull. Chem. Soc. Jpn.*, **2012**, *85*, 169–180.

(25) Kumagai, S.; Takaishi, S.; Iguchia, H.; Yamashita, M. Charge-bistable Pd(III)/Pd(II,IV) coordination polymers: phase transitions and their applications to optical properties, *Dalton Trans.*, **2015**, *44*, 8590–8599.

(26) Takaishi, S.; Kawakami, D.; Yamashita, M.; Sasaki, M.; Kajiwara, T.; Miyasaka, H.; Sugiura, K.; Wakabayashi, Y.; Sawa, H.; Matsuzaki, H.; Kishida, H.; Okamoto, H.; Watanabe, H.; Tanaka, H.; Marumoto, K.; Ito, H.; Kuroda, S. Dynamical valence fluctuation at the charge-density-wave phase boundary in iodide-bridged Pt compound $[Pt(chxn)_2I]I_2$, *J. Am. Chem. Soc.* **2006**, *128*, 6420–6425.

(27) Gerard, K. J.; Morgan, J.; Steel, P. J.; House, D. A. The synthesis, hydrolysis kinetics and structures of nickel(II) and cobalt(III) complexes of meso and racemic 1,2-diaminocyclohexane, *Inorg. Chim. Acta* **1997**, *260*, 27–34.

(28) Takaishi, S.; Yamashita, M.; Matsuzaki, H.; Okamoto, H.; Tanaka, H.; Kuroda, S.; Goto, A.; Shimizu, T.; Takenobu, T.; Iwasa, Y. One-dimensional bromo-bridged Ni^{III} complexes $[Ni(S,S\text{-}bn)_2Br]Br_2$ (*S,S*-bn=2*S*,3*S*-diaminobutane): synthesis, physical properties, and electrostatic carrier

doping, *Chem. Eur. J.* **2008**, *14*, 472–477.

(29) Mandal, P.; Lin, C.-H.; Brandão, P.; Mal, D.; Felix, V.; Pratihar, J. L. Synthesis, characterization, structure and catalytic activity of (NNN) tridentate azo-imine nickel(II), palladium(II) and platinum(II) complexes, *Polyhedron* **2016**, *106*, 171–177.

(30) Taylor, G. The phase problem, *Acta Cryst.* **2003**, *D59*, 1881–1890.

(31) (a) Dolomanov, O. V.; Bourhis, L. J.; Gildea, R. J.; Howard, J. A. K.; Puschmann, H. OLEX2: a complete structure solution, refinement and analysis program, *J. Appl. Crystallogr*. **2009**, *42*, 339–341; (b) Sheldrick, G. M. SHELXT - Integrated space-group and crystal-structure determination, *Acta Crystallogr., Sect. A: Found. Adv*. **2015**, *A71*, 3–8; (c) Sheldrick, G. M. Crystal structure refinement with SHELXL, *Acta Crystallogr., Sect. C: Struct. Chem*. **2015**, *C71*, 3–8.

(32) Macrae, C. F.; Bruno, I. J.; Chisholm, J. A.; Edgington, P. R.; McCabe, P.; Pidcock, E.; Rodriguez-Monge, L.; Taylor, R.; van de Streek, J.; Wood, P. A. Mercury CSD 2.0 - new features for the visualization and investigation of crystal structures, *J. Appl. Cryst*. **2008**, *41*, 466–470.

(33) Yamashita, M.; Manabe, T.; Inoue, K.; Kawashima, T.; Okamoto, H.; Kitagawa, H.; Mitani, T.; Toriumi, K.; Miyamae, H.; Ikeda, R. Tuning of spin density wave strengths in quasi-one-dimensional halogen-bridged Ni^{III} complexes with strong electron correlations, $[Ni^{III}(chxn)_2X]Y_2$, *Inorg. Chem.* **1999**, *38*, 1894–1899.

(34) Okamoto, H.; Toriumi, K.; Mitani, T.; Yamashita, M. Optical and magnetic properties of the halogen-bridged metal complexes modified by hydrogen department bondings: {M(1*R*,2*R*-cyclohexanediamine)$_2$Br}Br (M =Pt, Pd, and Ni), *Phys. Rev. B* **1990**, *42*, 10381–10387.

(35) Okamoto, H.; Mitani, T.; Toriumi, K.; Yamashita, M. Control of CDW state in halogen-bridged metal complexes, *Mater. Sci. Eng*. **1992**, *B13*, L9–L14.

(36) Takaishi, S.; Takamura, M.; Kajiwara, T.; Miyasaka, H.; Yamashita, M.; Iwata, M.; Matsuzaki,

H.; Okamoto, H.; Tanaka, H.; Kuroda, S.; Nishikawa, H.; Oshio, H.; Kato, K.; Takata, M. Charge-density-wave to Mott-Hubbard phase transition in quasi-one-dimensional bromo-bridged Pd compounds, *J. Am. Chem. Soc.* **2008**, *130*, 12080–12084.

(37) Yoshida, T.; Takaishi, S.; Iguchi, H.; Okamoto, H.; Tanaka, H.; Kuroda, S.; Hosomi, Y.; Yoshida, S.; Shigekawa, H.; Kojima, T.; Ohtsu, H.; Kawano, M.; Breedlove, B. K.; Guérin, L.; Yamashita, M. Optically visible phase separation between Mott-Hubbard and charge-density-wave domains in a Pd-Br chain complex, *ChemistrySelect* **2016**, *2*, 259–263.

(38) (a) Gaussian 16W, Revision 1.1, Gaussian, Inc., Wallingford CT, 2016; (b) GaussView, Version 6.1.1, Semichem Inc., Shawnee Mission, KS, 2016.

(39) NIST computational chemistry comparison and benchmark database, NIST standard reference database number 101, Release 21, August 2020, Editor: Russell D. Johnson III, http://cccbdb.nist.gov/

(40) Wakizaka, M.; Iguchi, H.; Takaishi, S.; Yamashita, M. Surface ohmic conductivity on a mott insulator based on a one-dimensional bromide-bridged nickel(III) complex, *Chem. Asian. J.* **2021**, *16*, 2947–2951.

(41) Ozawa, Y.; Ikuno, T.; Amano, S.; Ida, T.; Ibaraki, A.; Kimura, K.; Toriumi, K. Electrocrystallization, crystal structure, and solid state properties of halogen-bridged one-dimensional compound, $\{[Ni(en)_2Br](ClO_4)_2\}_\infty$, having an elongated Ni···Ni distance, *Mol. Cryst. Liq. Cryst.* **1996**, *278*, 189–197.

(42) Szacilowski, K. T.; Xie, P.; Malkhasian, A. Y. S.; Heeg, M. J.; Udugala-Ganehenege, M. Y.; Wenger, L. E.; Endicott, J. F. Solid-state structures and magnetic properties of halide-bridged, face-to-face bis-nickel(II)-macrocyclic ligand complexes: ligand-mediated interchanges of electronic configuration, *Inorg. Chem*. **2005**, *44*, 6019–6033.

(43) Lee, P. A.; Nagaosa, N.; Wen, X.-G. Doping a mott insulator: physics of high-temperature

superconductivity, *Rev. Mod. Phys.* **2006**, *78*, 17–85.

(44) S. S. Eaton, K. M. More, B. M. Sawant, G. R. Eaton, Use of the EPR half-field transition to determine the interspin distance and the orientation of the interspin vector in systems with two unpaired electrons, *J. Am. Chem. Soc.* **1983**, *105*, 6560–6567.

(45) V. B. Arion, V. Ch. Kravtsov, J. I. Gradinaru, Y. A. Simonov, N. V. Gerbeleu, J. Lipkowski, J.-P. Wignacourt, H. Vezin, O. Mentré, Potassium-controlled synthesis of heterotopic macrocycles based on isothiosemicarbazide, *Inorg. Chim. Acta* **2002**, *328*, 123–133.

(46) J. A. Weil and J. R. Bolton, Electron paramagnetic resonance: elementary theory and practical applications, 2nd Ed., John Wiley & Sons, Inc., Hoboken, 2007, Chapter 6.

(47) Tanaka, H.; Marumoto, K.; Kuroda, S.; Manabe, T.; Yamashita, M. ESR detection of induced spin moments in halogen-bridged mixed-metal complexes $Ni_{1-x}Pd_x(chxn)_2Br_3$, *J. Phys. Soc. Jpn*. **2002**, *71*,1370–1375.

(48) Sasaki, M.; Takaishi, S.; Miyasaka, H.; Sugiura, K.; Yamashita, M. Direct observation of the disorder of the methyl group of (*R*)-1,2-diaminopropane ligand in the quasi-1D bromo-bridged Ni(III) complex by STM, *J. Am. Chem. Soc.* **2005**, *127*, 14958–14959.

For TOC Only

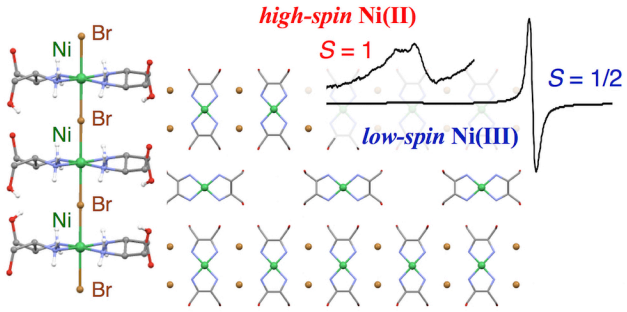

An intermediate state between the Mott–Hubbard and charge-density-wave states in an Ni-based MX-Chain was demonstrated. The Ni sites were mixed-valence, with high-spin Ni(II) and low-spin Ni(III) sites. This finding represents a new structural and electronic state of one-dimensional electronic systems.